Nanoscale

Accepted Manuscript

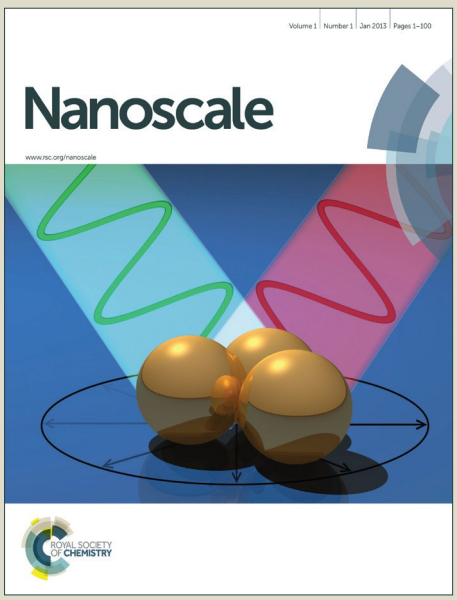

ROYAL SOCIETY OF CHEMISTRY

www.rsc.org/nanoscale

Journal Name

ARTICLE TYPE

Cite this: DOI: 10.1039/xxxxxxxxxx

Fabrication of poly-crystalline Si-based Mie resonators *via* amorphous Si on SiO_2 dewetting

Meher Naffouti,[ab] Thomas David,[a] Abdelmalek Benkouider,[a] Luc Favre,[a] Antoine Ronda,[a] Isabelle Berbezier,[a] Sebastien Bidault,[c] Nicolas Bonod[d] and Marco Abbarchi*[d]

Received Date
Accepted Date

DOI: 10.1039/xxxxxxxxxx

www.rsc.org/journalname

We report on the fabrication of Si-based dielectric Mie resonators *via* a low cost process based on solid-state dewetting of ultra-thin amorphous Si on SiO_2. We investigate the dewetting dynamics of a few nanometers layers annealed at high temperature to form submicrometric Si-particles. Morphological and structural characterization reveal the polycrystalline nature of the semiconductor matrix as well as rather irregular morphologies of the dewetted islands. Optical dark field imaging and spectroscopy measurements of single islands reveal pronounced resonant scattering at visible frequencies. The linewidth of the low-order modes can be ~20 nm in full width at half maximum, leading to a quality factor Q exceeding 25. These values reach the state-of-the-art ones obtained for monocrystalline Mie resonators. The simplicity of the dewetting process and its cost-effectiveness opens the route to exploiting it over large scales for applications in silicon-based photonics.

1 Introduction

Dielectric particles exhibiting resonant Mie scattering have been under investigation in the last few years owing to their remarkable optical properties in the visible and near-infrared wavelength range.[1–14] Similar to the metallic counterpart, these sub-micrometric particles feature pronounced resonant electromagnetic modes theoretically predicted[1,2] and experimentally demonstrated[3–14] in recent years for dielectric particles with sufficiently large refractive index ($n > 2.6$). Dielectric Mie resonators (MRs) represent a promising resource for light manipulation at the nanoscale and, due to their lower optical losses with respect to plasmonic resonators[15] and better compatibility with nowadays silicon technology (e.g. MOS transistors and photovoltaics), may overcome the performances of conventional metallic particles in the visible and near infrared spectrum.[4,12] Practical and cost-effective fabrication methods are thus needed for a realistic exploitation of this novel class of dielectric, optical devices.[10]

State-of-art MRs have been usually fabricated by top-down approaches,[4,6] nevertheless, silicon colloids[16] and nanosphere lithography[12] have been demonstrated adapted to implement complex optical functions such Fano-like lineshapes,[11] light detection[8] and perfect reflection. Another viable alternative for MRs fabrication is solid-state dewetting of ultra-thin monocrystalline silicon on insulator substrates (UT-SOI), recently proposed as a valid alternative to top-down methods.[9]

Commercial UT-SOI are provided only for few specifications of the top Si layer thickness h_0 which may limit the extension of this method for larger operating wavelength. Nonetheless, the commercially available UT-SOI are provided in a limited variety of underlying SiO_2 layer thickness. To dispense with costly UT-SOI technology and increase the versatility of this dewetting approach, we extend it to thin amorphous silicon films deposited on an arbitrary silica substrate.

Solid state dewetting has been exploited for the fabrication of polymeric, metallic, and semiconducting particles as it occurs in isotropic (e.g. amorphous) and anisotropic (e.g. crys-

[a] CNRS, Aix-Marseille Université, Centrale Marseille, IM2NP, UMR 7334, Campus de St. Jérôme, 13397 Marseille, France
[b] Laboratoire de Micro-Optoélectroniques et Nanostructures, Faculté des Sciences de Monastir, Université de Monastir, Monastir 5019, Tunisie.
[c] ESPCI ParisTech, PSL Research University, CNRS, 1 rue Jussieu, F-75005 Paris, France.
[d] CNRS, Aix-Marseille Université, Centrale Marseille, Institut Fresnel, UMR 7249, Campus de St. Jérôme, 13397 Marseille, France.
[d] CNRS, Aix-Marseille Université, Centrale Marseille, Institut Fresnel, UMR 7249, Campus de St. Jérôme, 13397 Marseille, France.
* marco.abbarchi@im2np.fr

talline) thin layers when heated well below their melting temperature.[17,18] In monocrystalline silicon (c-Si) dewetting evolves *via* hole-formation (initiated in presence of layer defects and impurities) followed by film retraction through a Rayleigh-like instability (rim formation associated to fingering) and finally, onset of monocrystalline islands.[9,19–23] In this case, due to the anisotropy of the semiconductor matrix, the Rayleigh-like instability leads to a partial self-ordering of the monocrystalline islands resulting in typical periodicities of the inter-particle distance. When using an amorphous Si layer (a-Si) instead, the effect of the thermal processing is twofold: crystallization of the a-Si in polycrystalline Si (p-Si) and film dewetting.[24–26] A relevant difference with respect to the crystalline case is the completely disordered organization of the island position and a rather large size dispersion.

Remarkably, the dewetting temperature and annealing time are largely reduced for amorphous layers with respect to the crystalline counterpart (e.g. a-Si can be dewetted at temperature lower than 600 ° C and a-Ge lower than 300 ° C while annealing for only 30 minutes[24–26]). The importance of this observation relies in the compatibility of low-temperature processing with back-end processing of C-MOS circuitry. Nevertheless, using c-Si[9,20,21] or a-Si[24–26] has several consequences on the dewetting dynamics and on the final features of the dewetted particles (e.g. grains and lattice disorder in p-Si islands), potentially affecting their optical properties. As an example, the changes in the Mie resonances induced by the transition from amorphous to crystalline silicon was studied in reference[13] showing a blue shift and an increasing Q factor while evolving towards the crystalline phase. On the other side, a-Si was recently proposed as a good alternative to c-Si for the implementation of all-optical switches based on MRs, due to its faster carrier relaxation leading to more pronounced optical non-linearities.[27] Similar considerations hold for ring resonators made of p-Si which allows for a faster switching time with respect to similar devices made of c-Si.[28]

The disordered spatial arrangement and broad size distribution of the dewetted islands may be considered as a limit of this approach if precise positioning is required (e.g. for the realization of high reflectivity mirrors[12]). On the other side, disordered systems can be exploited for light coupling with the substrate[29,30] suggesting that solid state dewetting could be efficiently used as a fabrication method of thin-film anti-reflection coatings[4].

Here we investigate the resonant scattering of sub-micrometric p-Si islands formed by dewetting a thin a-Si layer deposited in ultra-high vacuum on SiO_2 by molecular beam epitaxy (MBE). Size, shape and crystallinity of the dewetted islands are investigated *via* high resolution scanning electron microscopy (SEM), transmission electron microscopy (TEM) and atomic force microscopy (AFM). Dark field microscopy and spectroscopy measurements on samples with appropriate particle size and density revealed marked spectral features attributed to Mie modes. The 200-300 nm large Si particles exhibit two or three optical resonances, some of which with relatively sharp linewidth (we can find resonances of ∼20 nm in full width at half maximum (FWHM) corresponding to a quality factor Q >25, with $Q=\lambda_C/FWHM$ where λ_C is the central resonant wavelength).

Results and discussion

We produced *via* solid state dewetting 4 samples with different a-Si and SiO_2 thicknesses. The first 3 (labeled I, II, III) were used for investigating the dewetting dynamics and the last one (labeled IV) for the implementation of Mie resonators. The fabrication process is schematically reported in Fig.1 a) from panel 1 to 5: the Si(001) wafer (1) is oxidized by rapid thermal oxidation (RTO) under O_2 at 1000° C, (2). These conditions were calibrated to obtain a 6 nm SiO_2 thickness for samples I, II and III, and 145 nm for sample IV (this latter value matches that of commercial UT-SOI previously investigated in[9] providing a consistent basis for a valid spectroscopic comparison between the two configurations[7]). After chemical cleaning, the samples were transferred under clean-room atmosphere to the MBE chamber in ultra-high vacuum (UHV, $\sim 10^{-10}$ Torr) where a-Si was deposited at room temperature (3)). The thickness of the a-Si layer h_0 was 1, 2, 3 and 7 nm respectively for samples I, II, III and IV. Dewetting (5)) occurs during *in situ* annealing at high temperature (725 ° C for 25 minutes for samples I, II and III; 780 ° C for 30 minutes for sample IV). The situation after this step can be well appreciated on the SEM images (Fig. 1 b)). A further modification of the dewetting dynamics is obtained by milling the thin a-Si layer before annealing (step (4), only for sample IV). Sample etching was performed *ex-situ* by liquid-metal ion-source focused ion beam (LMIS-FIB) in a Tescan LYRA1 XMH dual-beam workstation operating at 30 keV and a beam current of ∼ 20 pA. This LMIS-FIB is equipped with a ultrahigh resolution mass-filter FIB COBRA-type from Orsay Physics. Patterning was performed using AuGe alloy sources and selecting a single element. In this study the sample was milled with Ge^+ ions that avoid sample contamination even if using Au^+ or Ge^+ ions is equally possible[9]. We etched *ex situ* only sample IV with several patterns (such as lines, squares and dot arrays).

SEM microscopy (Fig.1 b)) is used to investigate the size of the dewetted particles (see Fig.1 c)). They exhibit a linear dependence of their base size b as a function of the initial a-Si layer thickness h_0 (see Fig. 1 d)). This is similar to what was previously shown for c-Si[20] where $b \simeq 20h_0$ while in the present case of a-Si $b \simeq 12h_0$. The difference in the dependence of b on h_0 for a-Si and c-Si can be partially explained by a systematic under-estimation of the particle diameters for high density samples and small objects (Fig.1 b)). Nonetheless, it could be also explained by the different dewetting dynamics leading, for instance, to changes in the final equilibrium shapes as recently suggested.[26,31] We also

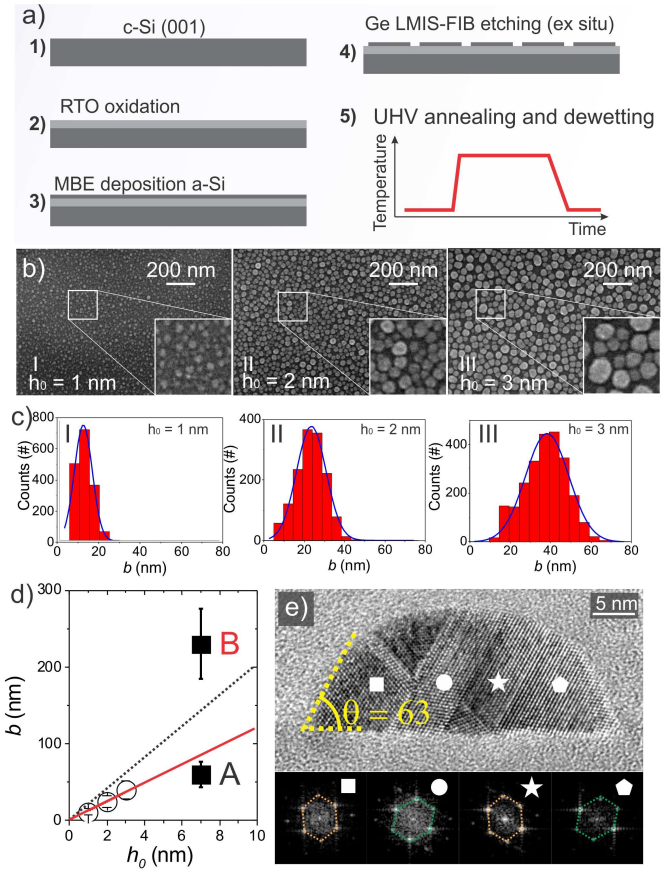

Fig. 1 a) Fabrication scheme: 1) c-Si (001) substrate; 2) RTO annealing and creation of a SiO_2 layer (6 nm thick for sample I-III, and 145 nm for sample IV); 3) room-temperature MBE deposition of a-Si (h_0 = 1,2 and 3 nm respectively for samples I, II and III; 7 nm for sample IV); 4) LMIS-FIB milling (only for sample IV); annealing UHV atmosphere at 725 ° C for 25 minutes for samples I, II and III, and 780 ° C for 30 minutes for sample IV. b) and c) SEM images and statistical distribution of base size b of sample I, II and III are respectively shown from the left to the right panel. Continuous lines are Gaussian envelopes of the statistical distributions. d) Data summary of samples I, II and III (open circles) and corresponding linear fit (red line). The black line shows the dependence shown in[20]. Full black squares are measurements from sample IV (see the dedicated section and Fig.2), A and B refers to different zones in the LMIS-FIB patterned areas. The error bars correspond to the standard deviation of the statistical distribution. e) High resolution TEM image of a dewetted island from sample III. The contact angle θ is highlighted. The bottom insets show the Fourier transform of the crystalline lattice in four distinct points of the island.

note that for these small values of h_0, we do not find evidence of a bimodal size distribution of b.[24,25]

From TEM measurements (see Fig.1 e)) we deduce a contact angle $\theta \sim 63$ degrees and a vertical aspect ratio $\eta \sim 0.4$ ($\eta = H/b$, where H is the particle height),[26,31] rather larger with respect to that found in c-Si islands where $\eta \sim 0.2$.[9] Regarding the crystalline structure of the dewetted islands we observe multiple stacking faults (twins) of large crystalline domains featuring differently oriented axes (see the bottom insets of Fig.1 e) where the Fourier Transform of the lattice is shown) confirming the polycrystallinity character of these objects.

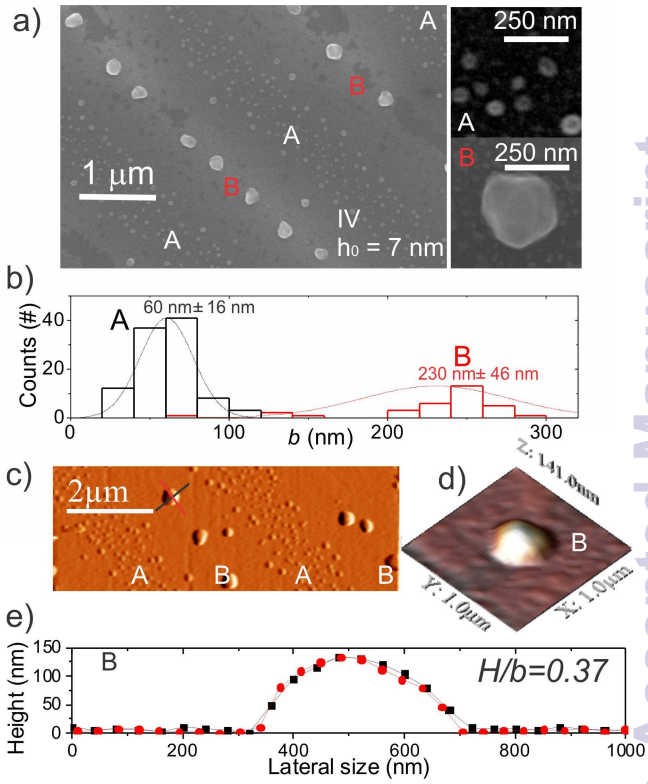

Fig. 2 a) SEM image of a patterned area (parallel lines spaced by 2.5 μm) after dewetting. A and B highlight respectively the areas with small and large islands. On the right, the two insets show enlarged views of islands from the A (top) and B (bottom) region. b) Statistical distribution of large and small islands shown in b). The continuous lines are Gaussian profiles. c) AFM image of a patterned area on sample IV. Continuous lines highlight the height profiles shown in e). d) 3D representation of the island highlighted in c) from zone B. e) AFM profiles extracted from zone B in c).

The lowest order mode of Si-based MRs is a magnetic dipole resonance which is observed for spherical particles with a diameter D typically larger than 100 nm (under the condition $D = \lambda_{res}/n_{Si}$ where λ_{res} is the central resonant wavelength and n_{Si} is the refractive index of silicon).[5] In order to obtain large enough particles capable of sustaining pronounced Mie modes at visible frequencies, we choose a $h_0 = 7$ nm (sample IV). Nevertheless, for spontaneously dewetted particles, the surface density is extremely large (e.g. $\sim 10^{10}$ cm^{-2} for $h_0 = 20$ nm in reference[31]) and impede the possibility to address individual objects by conventional confocal optical microscopy and spectroscopy. For that

purpose, the 7 nm a-Si layer is milled by LMIS-FIB providing additional control over particle size and organization.[9,20–22,32] In these conditions, the final result is a partially dewetted surface with a few large islands (not shown) and several islands formed within the patterns (see a SEM image in Fig.2 a) where the case of parallel lines etched in steps of 2.5 μm is shown).

A pronounced bimodal size distribution[24,25] is observed for this larger initial h_0 thickness: larger islands are organized along lines (zone B in Fig.2) and smaller islands are found in between (zone A in Fig.2). For the sake of thoroughness we mention that the smaller islands are found at least at a distance of ∼500 nm from the larger ones. A statistical investigation of the particles size from the two areas highlights their difference leading to non-overlapping distributions with average values 230 ± 46 nm in B and 60 ± 16 nm in A (the error represents the standard deviation). It is worth noting that, differently from the spontaneous dewetting case, where large and small islands are mixed,[24,25] this LMIS-FIB-assisted dewetting allows to spatially separate the two families while dramatically enhancing their difference in size. Concerning the larger particles in zone B (which are the only exhibiting resonant scattering as shown below), analyzing several lines, we observe a typical inter-islands spacing of about $D_{CC} \simeq$ 750 ± 150 nm (where D_{CC} is the center-to-center distance and the error represents the standard deviation).

Atomic force microscopy investigation of a particle from zone B (see Fig.2 c)-e)) reveals a height H = 130 nm and a base b = 355 nm providing a vertical aspect ratio η = 0.37 in good agreement with the TEM analysis (see Fig.1 e)). The shape of Mie resonators has a strong influence on their optical properties[33]. In particular, the vertical aspect ratio plays an important role in determining the spectral separation and the linewidth of electric and magnetic dipolar resonances as well as in controlling the onset of a quadrupolar mode[7]. In this sense the dewetting a-Si is an advantage with respect to c-Si as it enables for a largely increased η. Additional control over particles shape can be obtained by adding a few germanium monolayers: SiGe-based islands can be fabricated with an $\eta \simeq 1$ and improved in-plane symmetry[34] thus matching the features of state-of-the-art dielectric particles obtained by top-down methods.

We observe that the LMIS-FIB patterning allows to partially control the final particle size compared to what was expected with spontaneous dewetting (see Fig. 1 d) where the diameter b of the islands from samples I-IV are compared). More homogeneous size and spacing could, in principle, be obtained with optimized dewetting conditions or more complex LMIS-FIB patterns. The main idea at the basis of patterning is engineering the dewetting front and precisely define the amount of material available in order to induce the formation of one or more particles within the pattern. This was shown in previous reports for amorphous silicon, germanium, silicon-germanium alloys layers as well as for crystalline silicon (see references[9,20,22]). Even if a precise island organization goes beyond the aim of this work, we mention that a hint about this possibility can be seen in Fig. 3 b) and c) (obtained with a commercial LEICA DMI5000M microscope in dark-field configuration at 100× magnification): The scattering colours from the particles fabricated in the two different patterns (respectively squares and lines) are quite different due to their different particles average size. This patterning method was so far demonstrated on limited portions of the samples but it could, in principle, be extended over larger extensions. For that purpose adopting different etching techniques (e.g. interferential lithography[35]) would enable to obtain regular arrangement over inches scale.

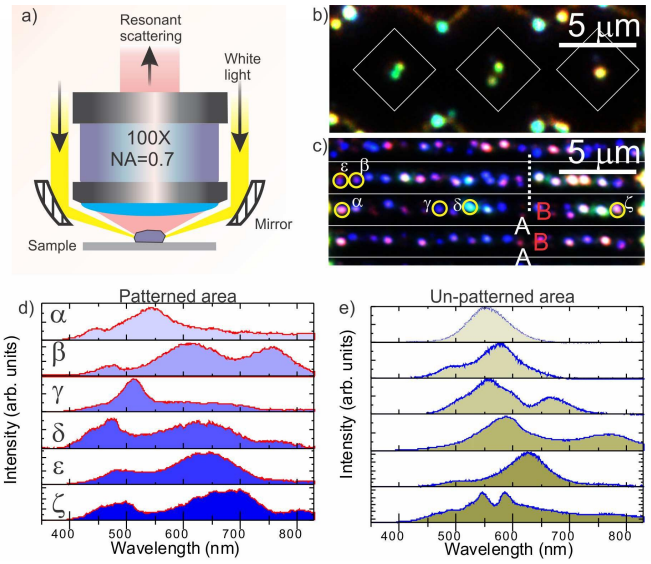

Fig. 3 a) Scheme of the excitation/collection method for DF imaging and spectroscopy of individual islands. b) DF image of 3 repetition of etched diamonds (3.5 μm × 3.5 μm) after dewetting of sample IV. The white lines highlight the LMIS-FIB pattern. c) 2.5 μm spaced lines pattern. α-ζ highlight the particles selected for spectroscopy shown in d). The yellow circles of 1 μm in diameter highlight the lateral resolution of the confocal microscope used for spectroscopic measurements. d) DF spectra of particles selected from c) and e) from non-patterned areas.

In sample IV the density of particles allows to measure the light scattering of individual islands and analyze them by dark-field (DF) spectroscopy performed with a home-made confocal microscope (see Fig.3 a) where a scheme describing the illumination and collection condition for DF spectroscopy is displayed). Under white light illumination with a large incident angle (70 degrees with respect to the normal to the sample surface), the resonant scattering is collected by a large numerical aperture 50× objective lens (NA = 0.70). Despite a diffraction-limited lateral resolution of ∼1 μm (determined by the objective's NA and by the size of the confocal spatial filter, a 50 μm multi-mode optical

fiber) the patterning enables to distinguish individual objects (see Figs.3 b) and c) where the cases of etched diamond patterns (3.5 μm $\times$ 3.5 μm) and parallel lines (2.5 μm spacing as in Fig.2) are displayed). These kinds of issues do not apply to the partially dewetted areas where D_{CC} is of the order of $\sim$10 μm or larger (not shown). Dark field spectra are obtained by sending the fiber-coupled light to an imaging spectrometer (30 cm focal length, 300 g/mm grating) and to a Si-based CCD camera providing a spectral resolution of about 0.6 nm in FWHM.

The bright and colorful DF images account for the formation of resonant modes in each large particle from zone B and a highly directional redistribution of the incident light. On the contrary, no light scattering occurs from zone A suggesting that the size associated to the corresponding particles ($H \simeq 30$ nm from AFM measurements, not shown) is too small to sustain resonant modes. For this reason we disregard the smaller particles in the following analysis.

A more precise insight on the resonant scattering properties is provided by the DF spectra of individual islands from zone B and from un-patterned areas of sample IV (see Figs. 3 d) and e) respectively). As already reported for the c-Si counterpart,[9] individual dewetted particles having a diameter of $\sim$300-400 nm exhibit pronounced scattering features typically displaying two or three bands ranging from $\sim$400 to $\sim$800 nm in wavelength (see also Fig. 4 c) where the spectrum of c-Si particle is reported for comparison). As the scattering response of Mie resonators is dominated by their size, shape and the contrast between its dielectric index and the environment, the crystalline order (e.g. the presence of staking faults, see Fig.1 e)) of the silicon matrix seems to have a limited influence on the optical properties of Mie resonators. Thus c-Si and p-Si, having very similar refractive index at visible and near infrared frequencies,[36] lead to similar results in the resonant scattering spectra of MRs.

By fitting the scattering spectra of individual islands with multiple Lorentzian profiles (see Fig.4 a)) we typically find that, as for other kind of silicon-based Mie particles,[6] the sharper resonances in the spectrum occur at shorter wavelengths and correspond to higher order modes featuring a lower radiation damping (see Fig. 4 a)-c)). Carrying on this analysis for about 40 p-Si particles from patterned and un-patterned areas, we find that the corresponding Q-factor can exceed 25 while its average value is about 10 (see Fig.4 b)). These values are in the state of the art range and are not very different from those reported for low-order modes found in MRs fabricated *via* top-down methods[6] accounting for the good quality of these p-Si-based MRs.

Conclusions

Full-wafer scale dielectric MRs were fabricated using solid-state dewetting of an amorphous ultra-thin Si layer. The technique uses dewetting which occurs during thermal annealing and transforms a two dimensional a-Si layer in p-Si islands. This method avoids complex, expensive and polluting etching steps. More importantly, the annealing time is completely independent from the extension of the sample surface and for a-Si is typically much shorter than that used for c-Si. It can be implemented at lower temperature making our method a viable solution for the implementation of Mie resonators as C-MOS backend-compatible process. As this method does not rely on the Si crystallinity it relaxes the need for expensive commercial SOI and it can be implemented on different substrates covered by an arbitrary thick SiO_2 layer. Furthermore, an important feature specific of amorphous silicon dewetting is the large surface density of the islands (and so reduced inter-particle distance) which provides a good surface covering not easy to obtain with other methods.

Spectral analysis of individual Mie scatterers is achieved by designing specific patterns by LMIS-FIB for isolating single Si particles with sufficiently large sizes and reduced surface density. In analogy with the c-Si dewetting counterpart and conventional Si

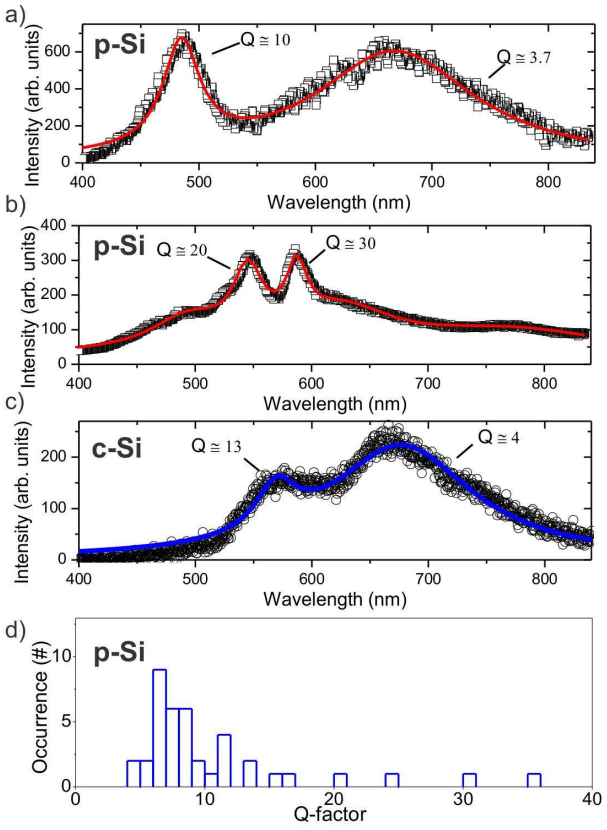

Fig. 4 a), (b)) Square symbols: DF spectrum of a p-Si island from a patterned (un-patterned) area. c) Same as a) and b) but for a c-Si island (see also reference[9]). e) Statistic of the Q factor for the sharpest resonance of 40 spectra obtained from patterned and un-patterned areas.

particles obtained *via* top-down approaches, this novel class of MRs features relatively narrow multi-polar modes rendering this fabrication method appealing for practical applications such as gas sensing[37] or photonic coupling with light emitters *via* Purcell effect.[38,39] Nonetheless, the strength of the method relies mostly in its scalability over large surfaces when spontaneous dewetting is used. In this sense, the method seems more appropriate for the fabrication of thin-film anti-reflection coatings[4]. To this end it must be recalled that the performances of a random organization of the scatterers can be comparable[29] or even overcome the ordered counterpart[30]. Finally, the method is very promising to study and manipulate light diffusion in complex scattering media[40–43].

2 Acknowledgments

We acknowledge the projects PHC MAGHREB (No. 32595SL), EMMAG- Erasmus Mundus Maghreb & Egypt. This work has been carried out thanks to the support of the A*MIDEX project (n° ANR-11-IDEX-0001-02) funded by the Investissements d'Avenir French Government program managed by the French National Research Agency (ANR).

References

1 A. B. Evlyukhin, C. Reinhardt, A. Seidel, B. S. Luk'yanchuk and B. N. Chichkov, *Physical Review B: Condensed Matter and Materials Physics*, 2010, **82**, 045404.

2 A. García-Etxarri, R. Gómez-Medina, L. S. Froufe-Pérez, C. López, L. Chantada, F. Scheffold, J. Aizpurua, M. Nieto-Vesperinas and J. J. Sáenz, *Optics express*, 2011, **19**, 4815–4826.

3 A. B. Evlyukhin, S. M. Novikov, U. Zywietz, R. L. Eriksen, C. Reinhardt, S. I. Bozhevolnyi and B. N. Chichkov, *Nano letters*, 2012, **12**, 3749–3755.

4 P. Spinelli, M. Verschuuren and A. Polman, *Nature Communications*, 2012, **3**, 692.

5 A. I. Kuznetsov, A. E. Miroshnichenko, Y. H. Fu, J. Zhang and B. LukâĂŹyanchuk, *Scientific reports*, 2012, **2**, year.

6 T. Coenen, J. van de Groep and A. Polman, *ACS nano*, 2013, **7**, 1689–1698.

7 J. van de Groep and A. Polman, *Optics express*, 2013, **21**, 26285–26302.

8 M. Garín, R. Fenollosa, R. Alcubilla, L. Shi, L. Marsal and F. Meseguer, *Nature communications*, 2014, **5**, year.

9 M. Abbarchi, M. Naffouti, B. Vial, A. Benkouider, L. Lermusiaux, L. Favre, A. Ronda, S. Bidault, I. Berbezier and N. Bonod, *ACS Nano*, 2014, **8**, 11181–11190.

10 G. Kang, J. Yoo, J. Ahn and K. Kim, *Nano Today*, 2015, **10**, 22–47.

11 J. Yan, P. Liu, Z. Lin, H. Wang, H. Chen, C. Wang and G. Yang, *ACS nano*, 2015, **9**, 2968–2980.

12 P. Moitra, B. A. Slovick, W. Li, I. I. Kravchenko, D. P. Briggs, S. Krishnamurthy and J. Valentine, *ACS Photonics*, 2015.

13 U. Zywietz, A. B. Evlyukhin, C. Reinhardt and B. N. Chichkov, *Nature communications*, 2014, **5**, year.

14 U. Zywietz, C. Reinhardt, A. B. Evlyukhin, T. Birr and B. N. Chichkov, *Applied Physics A*, 2014, **114**, 45–50.

15 J. B. Khurgin, *Nature nanotechnology*, 2015, **10**, 2–6.

16 L. Shi, T. U. Tuzer, R. Fenollosa and F. Meseguer, *Advanced materials*, 2012, **24**, 5934–5938.

17 J. Becker, G. Grün, R. Seemann, H. Mantz, K. Jacobs, K. R. Mecke and R. Blossey, *Nature Materials*, 2003, **2**, 59–63.

18 C. V. Thompson, *Annual Review of Materials Research*, 2012, **42**, 399–434.

19 E. Bussmann, F. Cheynis, F. Leroy, P. Müller and O. Pierre-Louis, *New Journal of Physics*, 2011, **13**, 043017.

20 M. Aouassa, I. Berbezier, L. Favre, A. Ronda, M. Bollani, R. Sordan, A. Delobbe and P. Sudraud, *Applied Physics Letters*, 2012, **101**, 013117.

21 M. Aouassa, L. Favre, A. Ronda, H. Maaref and I. Berbezier, *New Journal of Physics*, 2012, **14**, 063038.

22 I. Berbezier, M. Aouassa, A. Ronda, L. Favre, M. Bollani, R. Sordan, A. Delobbe and P. Sudraud, *Journal of Applied Physics*, 2013, **113**, 064908.

23 R. V. Zucker, G. H. Kim, W. C. Carter and C. V. Thompson, *Comptes Rendus Physique*, 2013, **14**, 564–577.

24 Y. Wakayama, T. Tagami and S. Tanaka, *Journal of applied physics*, 1999, **85**, 8492.

25 Y. Wakayama, T. Tagami and S.-i. Tanaka, *Thin Solid Films*, 1999, **350**, 300–307.

26 M. Korzec, M. Roczen, M. Schade, B. Wagner and B. Rech, *Journal of Applied Physics*, 2014, **115**, 074304.

27 M. R. Shcherbakov, P. Vabishchevich, A. Shorokhov, K. E. Chong, D.-Y. Choi, I. Staude, A. E. Miroshnichenko, D. N. Neshev, A. A. Fedyanin and Y. S. Kivshar, *Nano Letters*, 2015.

28 K. Preston, P. Dong, B. Schmidt and M. Lipson, *Applied Physics Letters*, 2008, **92**, 151104.

29 M.-C. van Lare and A. Polman, *ACS Photonics*, 2015, **2**, 822–831.

30 K. Vynck, M. Burresi, F. Riboli and D. S. Wiersma, *Nature materials*, 2012, **11**, 1017–1022.

31 M. Roczen, M. Schade, E. Malguth, G. Callsen, T. Barthel, O. Gref, J. A. Töfflinger, A. Schöpke, M. Schmidt and H. S. Leipner, *Applied Physics A*, 2012, **108**, 719–726.

32 A. Karmous, I. Berbezier and A. Ronda, *Physical Review B*, 2006, **73**, 075323.

33 A. B. Evlyukhin, C. Reinhardt and B. N. Chichkov, *Physical Review B: Condensed Matter and Materials Physics*, 2011, **84**,

235429.

34 P. Zhang, B. Yang, P. Rugheimer, M. Roberts, D. Savage, F. Liu and M. Lagally, *Journal of Physics D: Applied Physics*, 2009, **42**, 175309.

35 K. S. Kim, H. Jeong, M. S. Jeong and G. Y. Jung, *Advanced Functional Materials*, 2010, **20**, 3055–3063.

36 J. H. Ho, C. L. Lee, T. F. Lei and T. S. Chao, *J. Opt. Soc. Am. A*, 1990, **7**, 196–205.

37 A. Tittl, H. Giessen and N. Liu, *Nanophotonics*, 2014, **3**, 157–180.

38 B. Rolly, B. Bebey, S. Bidault, B. Stout and N. Bonod, *Physical Review B: Condensed Matter and Materials Physics*, 2012, **85**, 245432.

39 X. Zambrana-Puyalto and N. Bonod, *Physical Review B*, 2015, **91**, 195422.

40 L. Sapienza, H. Thyrrestrup, S. Stobbe, P. D. Garcia, S. Smolka and P. Lodahl, *Science*, 2010, **327**, 1352–1355.

41 T. Strudley, T. Zehender, C. Blejean, E. P. Bakkers and O. L. Muskens, *Nature Photonics*, 2013, **7**, 413–418.

42 D. S. Wiersma, *Nature Photonics*, 2013, **7**, 188–196.

43 F. Riboli, N. Caselli, S. Vignolini, F. Intonti, K. Vynck, P. Barthelemy, A. Gerardino, L. Balet, L. H. Li, A. Fiore *et al.*, *Nature materials*, 2014, **13**, 720–725.